Work function reduction in lanthanum hexaboride hollow cathodes operated in gas discharges

IEPC-2017-399

Presented at the 35th International Electric Propulsion Conference
Georgia Institute of Technology – Atlanta, Georgia – USA
October 8–12, 2017

Pablo Guerrero*
California Institute of Technology,Pasadena, CA 91125, USA

James Polk†
Jet Propulsion Laboratory, California Institute of Technology, Pasadena, CA 91109, USA

Matthias H. Richter‡
California Institute of Technology, Pasadena, CA 91125, USA

and

Alejandro Lopez Ortega§
Jet Propulsion Laboratory, California Institute of Technology, Pasadena, CA 91109, USA

Abstract: Thermal characterization of lanthanum hexaboride (LaB_6) hollow cathodes has revealed lower than expected electron emitter temperatures when the cathode reaches steady state. This phenomenon is observed at discharge currents ranging from 5 to 35 A and xenon mass flow rates of 5 to 25 sccm in cathodes with three different orifice diameters. Thus, the accepted value of the work function for polycrystalline LaB_6, 2.66 eV, does not describe well the emission characteristics of LaB_6 hollow cathodes operating with internal gas discharges at steady state. The measured temperatures and a model of the hollow cathode emitter and xenon discharge were used to estimate the value of the work function in these experiments, yielding a value ranging from 2.1 - 2.44 eV. Measurements of the work function as a function of depth on a hollow cathode emitter using X-ray photoelectron spectroscopy and ion beam milling indicate that the work function in a thin layer near the emitting surface is lower than in the bulk material. We postulate that a lanthanum-rich emitting surface with a lower work function develops as a result of lanthanum recycling in the internal plasma.

*GALCIT, Aerospace Department, pguerrer@caltech.edu
†Principal Engineer, Propulsion, Thermal, and Materials Engineering Section, james.e.polk@jpl.nasa.gov
‡Joint Center for Artificial Photosynthesis, Division of Chemistry and Chemical Engineering, mrichter@caltech.edu
§Member of the Technical Staff, Electric Propulsion Group, alejandro.lopez.ortega@jpl.nasa.gov

Nomenclature

J_D	= Cathode net discharge current
V_D	= Cathode net discharge voltage
T	= Temperature
$\dot{m}_{Xe}$	= Xenon mass flow rate
ϕ	= work function
$\phi_{Schottky}$	= Schottky effect work function
λ	= mean free path
La	= Lanthanum
B	= Boron
C	= Carbon
Ar	= Argon
TC	= Thermocouple
EDM	= Electro Discharge Machining

I. Introduction

NASA's vision for human exploration for the near future includes the proposed Deep Space Gateway (DSG) and Deep Space Transport (DST). One of the ultimate objectives is piloted Mars missions employing this architecture. However, this ambitious goal is extraordinarily difficult given the large mass necessary to reach Mars and provide habitable conditions for the astronauts. However, a very high efficiency propulsion system such as high power electric propulsion can yield mass reductions that enable near-term deep space missions. NASA is investing in high power, light weight solar arrays and high power Hall thruster systems to enable this vision. Reaching further with heavier payloads is the key objective of this new endeavor. In order to successfully accomplish this challenge, a new scalable propulsion system has been under development at NASA since 2012. The development effort is led by the NASA Glenn Research Center (GRC) and the Jet Propulsion Laboratory (JPL) and includes Aerojet Rocketdyne as an industrial partner. The goal is to develop the components for an Advanced Electric Propulsion System (AEPS) with a total system power of 40 kW. This could be applied initially to the DSG and is scalable to even higher power levels for the DST or other future applications. A key building block of the system is the Hall Effect Rocket with Magnetic Shielding (HERMeS). HERMeS' nominal operating power is 12.5kW of discharge power, with a specific impulse up to 3000 s and a service life of up to 50 kh.

Increased understanding of the detailed physical processes underlying Hall thruster operation has eliminated some of the possible failure modes that can limit the thruster lifetime. One example of a significant breakthrough in Hall thruster technology is the so-called magnetic shielding, a technique that employs carefully engineered magnetic fields to protect surfaces close to the plasma discharge from erosion. Nonetheless, a number of failure modes associated with different Hall thruster components are yet to be resolved, several of which are related to the thruster cathodes. It is important that HERMeS service life, aimed to exceed 50 kh, is not limited by the cathode lifetime. Thus, understanding cathode failure modes is of paramount importance for future NASA activities.

The current baseline cathode technology for the AEPS program is the barium dispenser cathode, which relies on a porous tungsten emitter impregnated with a barium-calcium-aluminate mixture that maintains a low work function surface complex of barium atoms on oxygen atoms adsorbed on the tungsten emitter surface. This type of cathode has demonstrated the capability for long life, but lanthanum hexaboride (LaB_6) hollow cathodes are a promising alternative that have also been under development. LaB_6 cathodes have also demonstrated the capability for long life, but are much less susceptible to poisoning by reactive gases than dispenser cathodes and scalable to extremely high power levels. LaB_6 emitter lifetime is ultimately limited by evaporation related to high temperature operation and thermal loads.

Thermionic electron emission is the principal mechanism upon which hollow cathode discharges operate [4]. The thermodynamic work necessary to free electrons from the cathode insert inner surface is determined by the emitting surface work function. The fraction of electrons in the emitter with sufficient energy to escape the work function barrier at the surface is exponentially related to the surface temperature. Thus, precise

knowledge of the emissive surface temperature distribution is essential to fully understand the behavior of thermionic emitting surfaces. In addition, insert evaporation, one of the main failure modes that affects state of the art cathodes, is also exponentially related to the material temperature.

In-depth understanding of the LaB_6 cathode performance requires an accurate determination of the temperature distribution of the insert inner surface. However, precise temperature measurements are challenging due to the high temperature at which these cathodes normally operate, often close to 2000 K. Further, LaB_6 cathodes consist of many components that cluster in assemblies, which makes them difficult to instrument. Previous efforts have established two approaches for measuring temperatures inside hollow cathodes, namely thermocouples and fiber optic pyrometers.

Type C commercial thermocouples have the highest temperature range of application (0-2320°C), which makes them an attractive option for cathode instrumentation. The downside is that they typically have a 1% precision. Fiber optic systems, on the other hand, require calibration, which can be very difficult to accomplish at that high temperature without using thermocouples.

In this paper, we present the results from using type C thermocouples to measure temperatures inside LaB_6 cathode inserts for a variety of cathode operating conditions and three different orifice diameters. Thermocouple accuracy and stability were assessed both experimentally and by computational simulations using the OrCa2D hollow cathode code and Comsol. Surprisingly, the data revealed that the commonly accepted work function value for polycrystalline LaB_6 (2.66eV[4]) cannot adequately describe the emissive characteristic of the cathode at steady state. Instead, lower work functions are necessary to fit the measured temperatures and discharge currents to the Richardson-Dushman equation. We propose that these atypically low work function values is a consequence of lanthanum redeposition on the emitter due to processes in the hollow cathode interior plasma. The lanthanum ionization mean free path is of the order of the cathode orifice diameter near the orifice plate, so a large fraction of the evaporated lanthanum atoms are likely ionized before they can escape. Ionized lanthanum can be driven back to the cathode emitting surfaces and can change the composition of the emitting surfaces towards lanthanum-rich stoichiometries, which could explain the abnormal work functions found in this work. A similar recycling effect for barium has been found in dispenser hollow cathodes as well, and makes their operation in gas discharges quite different from cathodes in vacuum devices[? ?].

II. Description of the measurement approach

The cathode used in these experiments has been described in the past. Briefly, it consists of a cathode tube with a LaB_6 insert positioned at the downstream end, right in front of the orifice plate (Fig. 1). The downstream portion of the cathode tube is surrounded by a heater utilized to preheat the insert material for ignition. The heater is covered by tantalum foil shielding to minimize heat loss through radiation at start or during normal operation. Finally, the assembly is enclosed in one more concentric electrode, termed the keeper, which is used as an ignitor electrode or to maintain a secondary discharge to keep the cathode operating in the event of extinction of the main discharge.

In this work, three orifice plates with different orifice diameters were used - small, medium and large. Medium refers to the nominal orifice plate envisioned for HERMeS, and the small and large orifice diameters were 80% and 160% of the nominal, respectively. The insert was perforated using electro-discharge machining (EDM) in order to place three 1.5875 mm Idaho Laboratories Type C thermocouples longitudinally. The thermocouples were distributed evenly in the azimuthal direction and were installed at three different depths in the insert (Fig. 2). Herein, we use TC1, TC2, and TC3 to refer to the temperatures measured by the thermocouples positioned at the highest, middle, and lowest depth, respectively (see Fig. 2). A second order polynomial was used to fit the three measurements to give an approximation of the temperature profile.

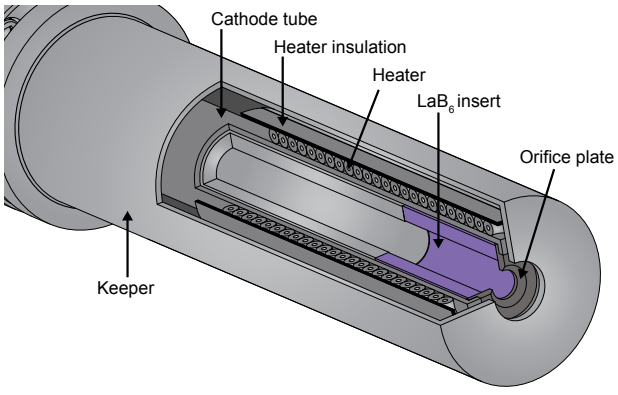

Figure 1: LaB_6 hollow cathode schematic.

A copper cylindrical anode 50.8 mm in diameter and 25.4 cm long was placed 19.56 mm from the keeper face, concentric with the assembly. Experiments were performed inside a 4m^3 stainless steel vacuum chamber equipped with two 10″cryopumps with base pressure 2e-7 Torr. Data were acquired using a custom built system based on a Opto22 SNAP-PAC-EB brain that measures voltages, currents, and xenon mass flow rates with a precision of 10 mV, 10 mA and 0.01 sccm, respectively, and a 2s refresh rate. Thermocouple signals were also acquired with the aforementioned equipment, which performs the cold junction temperature correction.

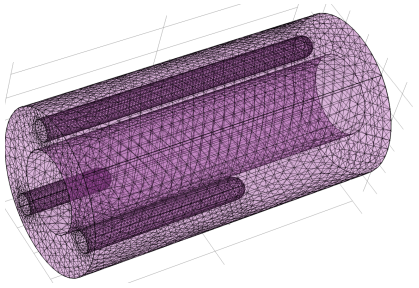

Figure 2: Insert finite element model with three EDM thermocouples wells.

III. Experimental Results

We initially sought to acquire the temperature distribution using the three thermocouple approach described above. When the cathode was set to a specific operating condition, a temperature transient was observed before the temperatures stabilized. Interestingly, we found that the duration of the transient is unpredictable and depends on the previous history of the cathode: if the cathode is in steady state and a small change to either J_D or $\dot{m}_{Xe}$ is applied, the cathode temperature, as determined by the thermocouples, adapts rapidly with only a few tens of degrees of overshoot or undershoot with respect to the steady state temperature that the cathode converges to over time. In such cases, the duration of the transient is around 30min to a few hours. A detailed description of the transient behavior is provided in the following section.

Due to the variation in the time required to reach steady state, and the large number of operating points to be tested, we developed an autonomous data acquisition and control (DAQ) strategy which determines when the cathode reaches steady state. The system defines steady state when the temperature difference in two consecutive 15min intervals is less than 1°C for all three thermocouples.

A. Transient behavior

1. *Initial start with a brand new LaB_6 insert*

Using the automatic DAQ setup described above, we first assessed the system behavior upon initial start with a brand new LaB_6 insert. The ignition was performed at J_D=25A and $\dot{m}_{Xe}$=14.75sccm. Data showed that for a new insert, temperatures take tens of hours to reach steady state (Fig. 3). After that long transient, we observed a small amplitude, low frequency periodic fluctuation in the measured temperatures. (This phenomenon is not fully resolved in Fig. 3).

In addition, the data showed a peak temperature of 1737°C and that the condition $\frac{\Delta T_{mean}}{\Delta t} = 0$ occurred around 65h after ignition, where T_{mean} is the mean temperature of all three thermocouples.

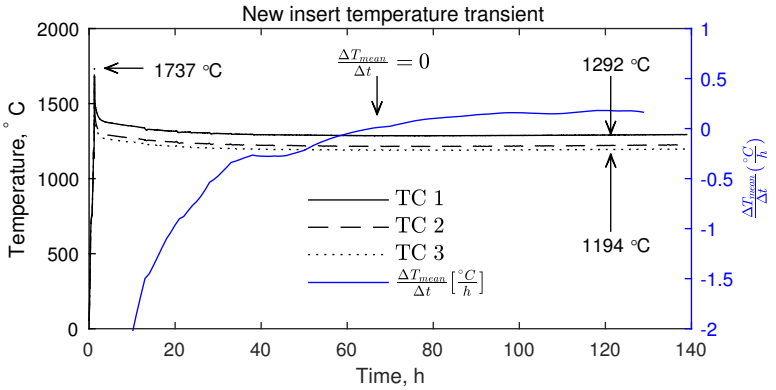

Figure 3: Thermal transient for a brand new insert at J_D=25A and $\dot{m}_{Xe}$=14.75sccm with the nominal orifice.

2. *Initial start after atmospheric exposure*

To further elucidate the unexpected cathode behavior, we studied the cathode thermal transients upon ignition after exposure to the atmosphere for several hours. To this end, we stopped the cathode discharge ($J_D = 0$) and let the cathode cool down completely (until thermocouples read ambient temperature) and then opened the vacuum chamber. After several hours, we evacuated the chamber and reignited the cathode with $J_D = 25A$ and $\dot{m}_{Xe} = 14.75sccm$. This re-ignition operation was performed manually, therefore, the temperature right before ignition is not

the same for the three cases shown in Fig. 4. Only TC1 is shown for each start, which typically is the hottest of all three at ignition.

As shown in Fig. 4, all three starts after atmospheric exposure had initial temperatures between 1459 and 1506 °C. There does not seem to be a clear relationship between temperature right before ignition and temperature right after ignition, although the coldest of this start reached the highest of the peak temperatures. A more carefully designed experiment is necessary to gain a further understanding of the thermal transient at ignition.

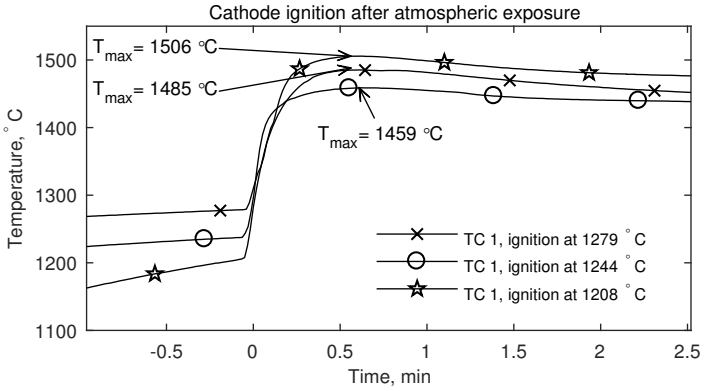

Figure 4: Thermal transient at J_D=25A and $\dot{m}_{Xe}$=13sccm with the nominal orifice after exposing the cathode to the atmosphere for several hours

3. Transients associated with hot re-ignitions

We define hot re-ignition as the process of igniting the cathode after a sudden shutdown (J_D=0), and allowing only a few hundred degrees cool-down before reigniting it. At that point, switching on only the keeper or the keeper and the heater might be necessary to regain ignition. Fig. 5 shows the temperature evolution during two different hot re-ignition experiments, synchronized at T=0.

It can be observed in Fig. 5 that before shutting down the cathode, neither of the experiments had reached steady state, i.e., there is a temperature difference of 26°C. Both experiments were performed with the nominal orifice plate and J_D=25A and $\dot{m}_{Xe}$=13sccm. As can be observed, when an attempt at re-ignition was made by shutting down the cathode and allowing it to cool down to 1229°C, the discharge re-ignited without a temperature overshoot. Later on, when the cathode was shut down and the temperature dropped to 1194°C, the cathode re-ignited and reached a peak temperature of 1410°C. A third hot re-ignition test was performed, reaching a minimum temperature of 864°C right before re-ignition, and the cathode TC1 peak temperature measured 1447°C.

4. Transients associated with discharge current step events

Finally, we tested the cathode behavior upon discharge current step events. To this end, we first ignited that cathode and allowed it to reach steady state, as determined by the DAQ system. At that point small changes in J_D of 2.5A were suddenly imposed. These changes in the discharge current were applied with both ascending and descending currents. The DAQ transitioned from one operating point to the next only when a steady state condition had been reached. The thermal transient associated with the step events is shown in Fig. 6. We observed that the direction of the discharge change (whether positive or negative) did not determine the direction of the temperature deviation with respect to the value that the temperature would ultimately reach at steady state. In some instances there was an overshoot (between 5A to 7.5A, 7.5A to 10A and 10A to 12.5A) whereas at others there was an undershoot

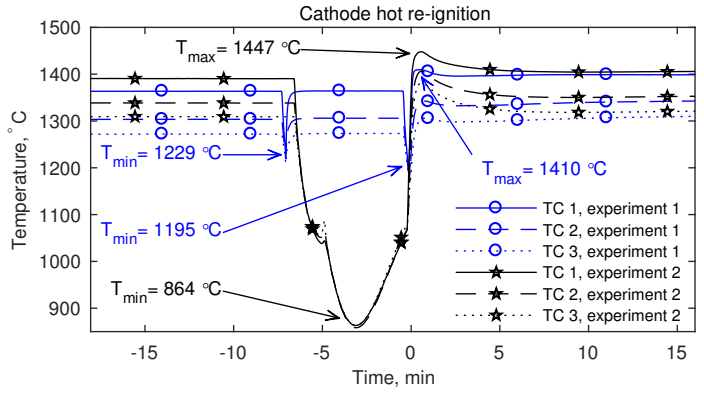

Figure 5: Thermal transient associated with hot re-ignition at J_D=25A and $\dot{m}_{Xe}$=13sccm with the nominal orifice. TC1 temperature shown for both experiments.

(between 15A to 17.5A and 17.5A to 20A). There is one case in which the temperature transitions with no over- or undershoot (12.5A to 15A), right in the middle of overshoot and undershoot trends.

5. Sudden change of steady state for one operating condition

In addition to the results above, experiments revealed one additional intriguing phenomenon. We observed that while running the cathode at fixed operating conditions, steady state temperatures changed from one start to the next (Fig. 7a). Following these experiments we found a ring of black deposit in the downstream region of the insert inner surface (Fig. 7b). When the deposit was removed, the steady state temperature dropped by almost 100°C. We hypothesized that the source of this black coating is a graphite cup located at the cathode downstream end. Thus, we replaced the graphite cup with a 0.001 thick tantalum cup and ran the cathode for tens of hours and several starts. Borescope inspection of the insert inner surface following these runs did not reveal any deposits, confirming that the source of the coating was indeed graphite. We propose that during cathode operation, carbon gets ionized and pushed by the electric field toward the insert inner surface, resulting in the observed deposit. As a 100°C increase in the insert temperature significantly impacts evaporation, and consequently the lifetime of the cathode, we suggest that graphite deposition has an important negative impact in the service life of the cathode. Our results strongly suggest that graphite cups be eliminated or at least redesigned in future cathode designs.

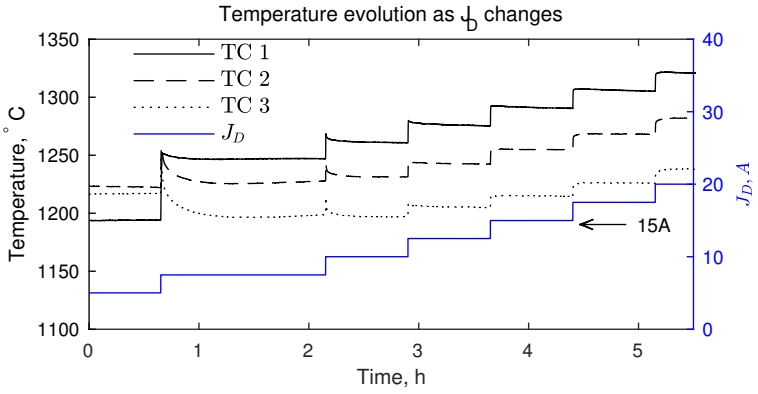

Figure 6: Thermal transient evolution with J_D at $\dot{m}_{Xe} = 10sccm$ with nominal orifice

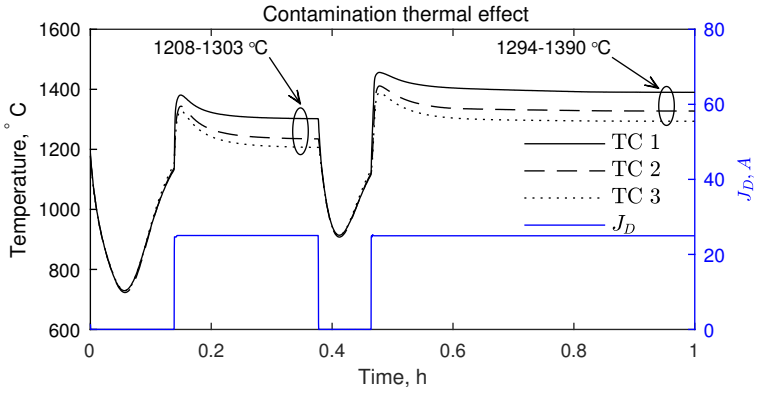

(a) Abnormal thermal transient after a hot re-ignition with the nominal orifice at J_D=25A and $\dot{m}_{Xe}$=14.75sccm.

(b) Detail of the contaminant deposited on the inside of the insert.

Figure 7: Abnormal steady state change

B. Steady state temperatures

The steady state temperature distribution of the cathode insert was obtained for each orifice diameter at discharge currents of 5,10,15,20,25,30, and 35A, and for each discharge current, $\dot{m}_{Xe}$ was set at 5,10,15,20 and 25 sccm. For the large orifice, the 5A case was not studied as the cathode was in plume mode for that condition over the whole $\dot{m}_{Xe}$ range under consideration. Temperature maps constructed from those data are shown in Fig. 8.

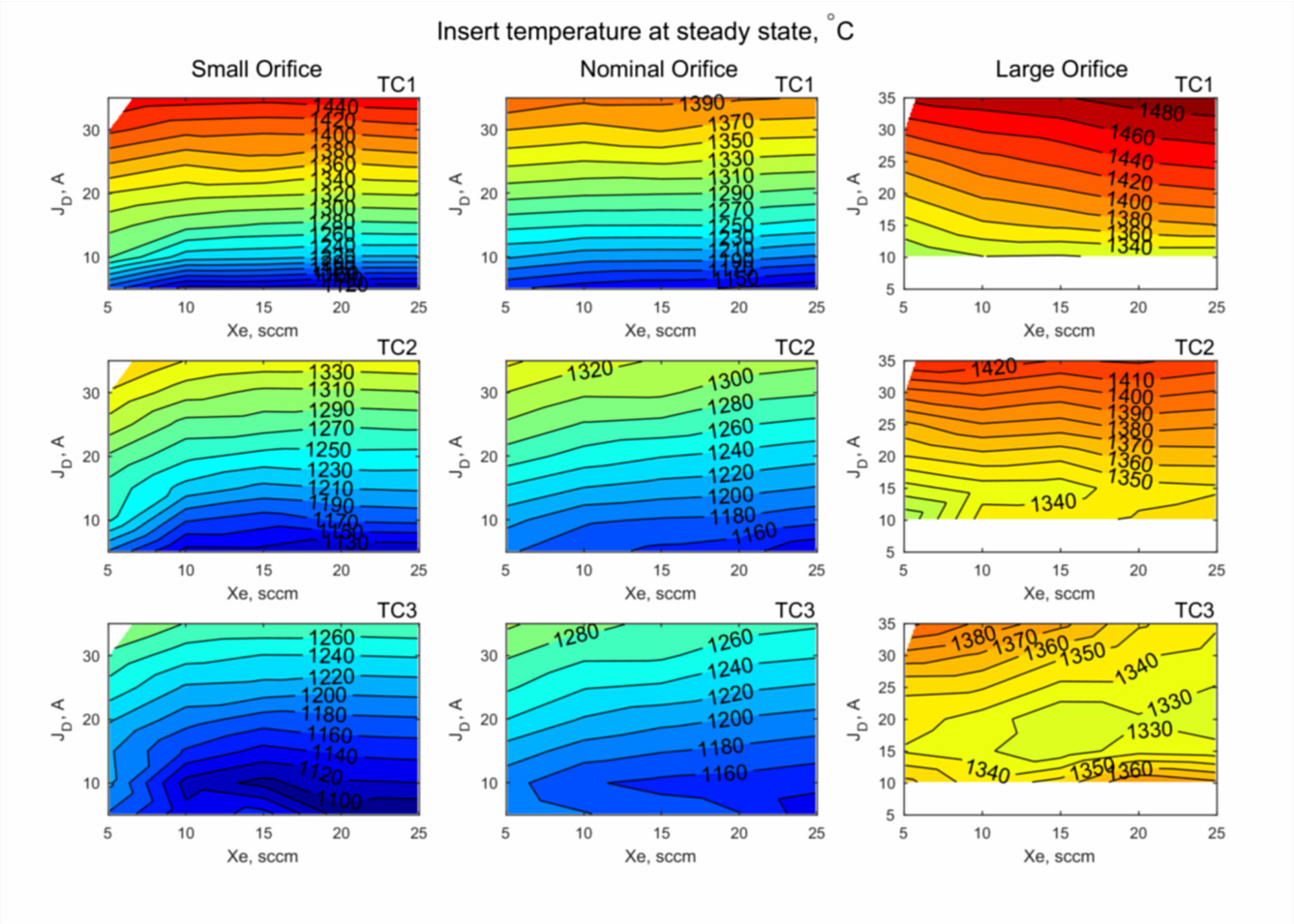

Figure 8: Steady state temperature distribution for each cathode configuration and each thermocouple.

IV. Discussion

A. Effect of orifice size on temperature

In order to assess which orifice configuration offers the best performance, we estimated the temperature profiles along the insert by fitting the data with a second degree polynomial (Fig. 9). As shown in the figure, the Large orifice configuration has the highest peak temperatures for every operating condition. This is not a desirable mode of operation, as it will evaporate the insert material faster for a given discharge current. The profiles for discharge current above $J_D = 15$A have the smallest difference between maximum and minimum temperatures for a given profile. Minimizing the temperature gradient along the axis of the insert is desirable because it should then erode more uniformly over thousands of hours. A more peaked temperature profile to wear through first in the location of peak temperature, leading to structural failure of the insert. Nonetheless, this is a consideration of lesser importance compared to minimizing the peak temperature for the same discharge current.

On the other hand, the small orifice shows the biggest temperature range over the same operating condition space. Peak temperatures are lower than for the big orifice case, but larger than for the nominal orifice size for discharge currents above 5A. Differences between maximum and minimum temperatures along the insert are the largest of the three configurations for all discharge currents above 5A.

The nominal orifice diameter offers the lowest temperature peaks for discharges above 5A and differences between maximum and minimum temperatures that lie between those of the larger and smaller orifices. This configuration is the most appealing one in terms of thermal distribution. In this analysis, the evolution of the insert inner diameter and consequent effect on the temperature profile has not been taken into consideration

when choosing the best configuration for the lifetime of the insert. That analysis would require knowledge of how the temperature profile evolves as the LaB_6 insert erodes.

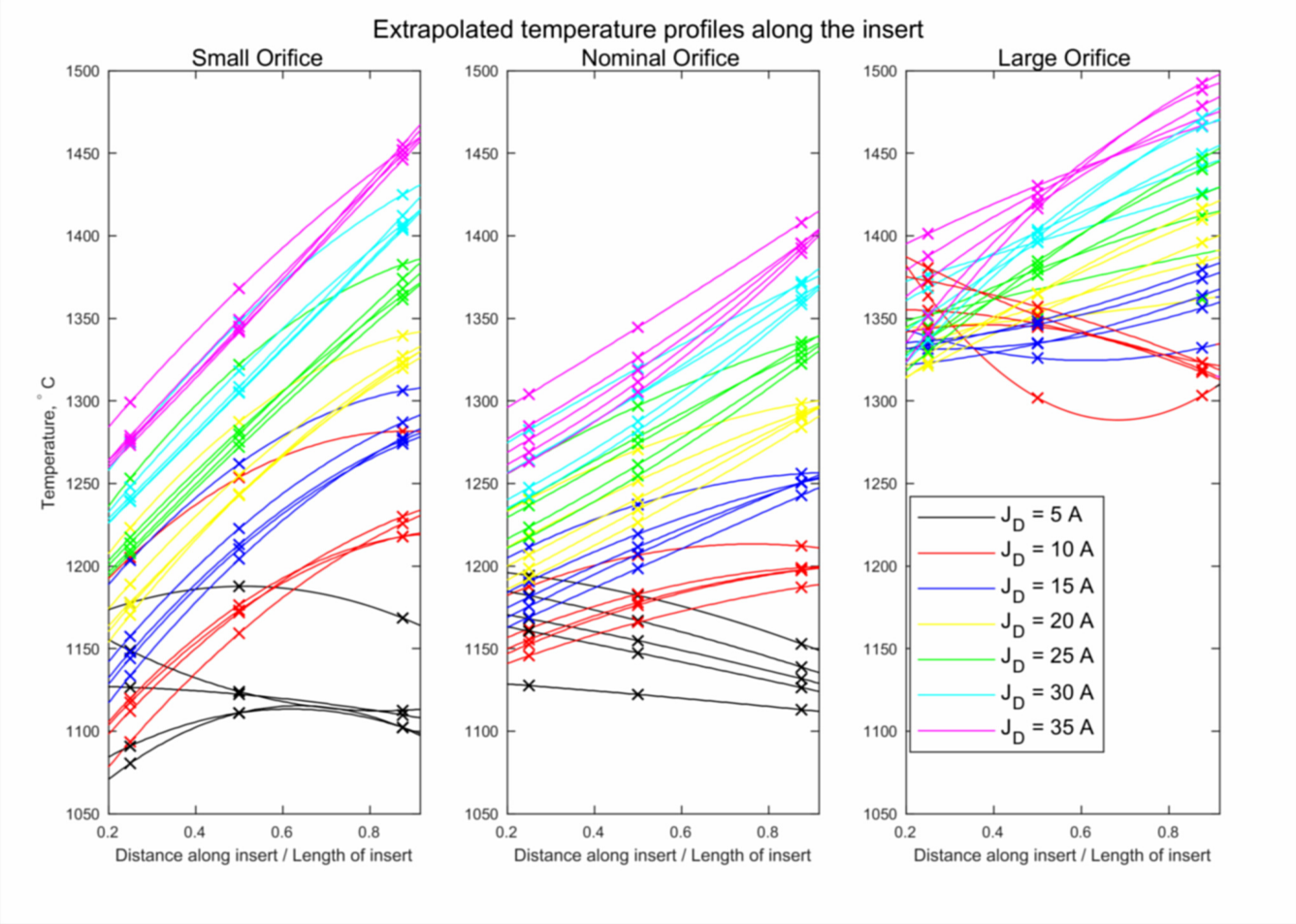

Figure 9: Temperature profiles approximated by a second degree polynomial fit to the thermocouple data for each operating condition .

B. Inferred work function

At every point on the insert emitting surface, the balance between the flux of emitted electrons and the flux of ions and electrons from the plasma back to the surface determines the net current density. Integrating these three components over the cathode area yields the total discharge current,

$$J_D = \iint_S (j_{ther}(\phi, X) - j_e(X) + j_i(X))\, dS, \tag{1}$$

where S is the insert emitting surface, X is a point in surface S, and $j_e(X)$ and $j_i(X)$ are the electron and ions density currents that return to the emitting surface and effectively increase and reduce the demand of electrons emitted (j_{ther}) for the same J_D respectively. j_{ther} is the thermionic emission current density as modeled by Richard-Dushman equation [4]

$$j_{ther}(\phi, X) = DT(X)^2 \exp\left(\frac{-e(\phi - \phi_{Schottky})}{k_B T(X)}\right) \tag{2}$$

with corrected parameter $D = 29A/cm^2K^2$ for work function temperature dependency. $T(X)$ is the temperature at any point X in S, k_B is Boltzmann constant. ϕ is the work function of the material with a nominal

value of 2.66eV for LaB_6, $\phi_{Schottky}$ is the reduction in the work function due to the external electric field, and e is the electron charge.

If we try to match Eq. 1 assuming $\phi_{Schottky} = 0\ eV$, zero ion or electrons return current, $\phi = 2.66\ eV$ and an axisymmetric temperature distribution from Fig.9, we realize that there is not enough emission to generate the measured discharge current J_D. Two terms help increase the net current to the cathode for the same temperature distribution, which have been neglected in this calculation. One of them is $\phi_{Schottky}$ which typically has a value on the order of 0.1 eV. Even considering that, the ion return current would have to be more than 50% of the discharge current to balance Eq. 1.

Therefore, we concluded that one possible explanation for this apparent lack of current capability could be explained if we assume that the work function in the material is lower than the value of 2.66eV. In the following subsections we will present 2 different estimates for the work function for every orifice size and operating condition.

1. Work function estimation, method 1: Matching net J_D

Computing the work function necessary to match J_D assuming $\phi_{Schottky}$, $j_e(X)$ and $j_i(X)$ are zero results in the distributions shown in Fig. 10. The evolution of the work function seems to follow a decreasing pattern with increasing discharge current until a minimum value at which point the trend is reversed and the work function increases. The effect of the $\dot{m}_{Xe}$ seems of lesser importance for higher than 15sccm flows. In the late 1970s, Storm and Mueller [8] reviewed all previous measurements of the work function for near-stoichiometry polycrystalline LaB_6 and found that the literature did not agree on one single value, but instead they defined a range of 2.52 to 2.87 eV which encompassed the measured values. The work function found with method 1 is far from this range for most of the operating conditions studied.

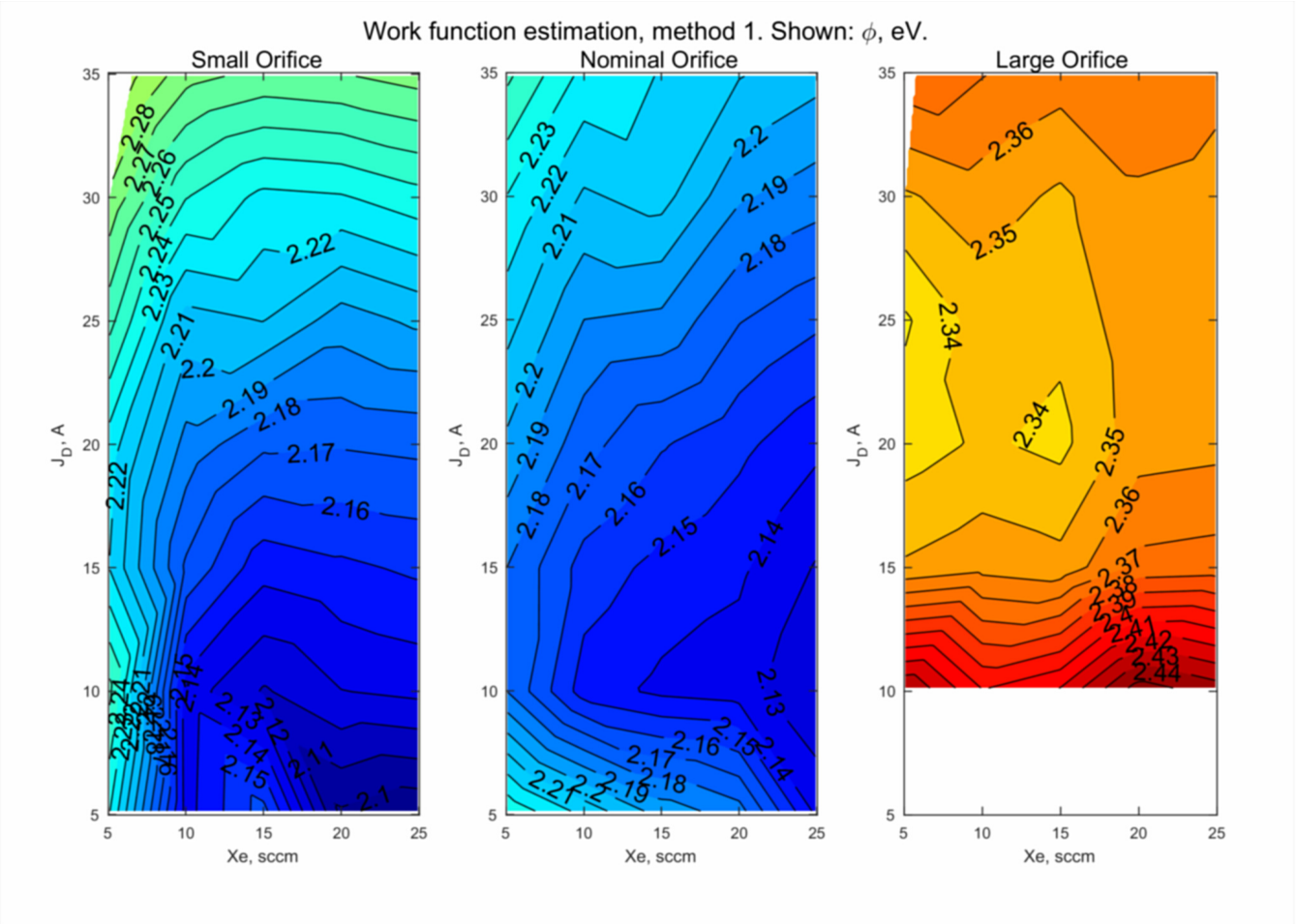

Figure 10: Computed work function with inferred insert temperature distribution, zero return current and $\phi_{Schottky} = 0$.

2. Work function estimation, method 2: Minimization of sum(abs($J_D(\phi) - J_{D,measured}$)) per orifice.

If we assume that $\phi_{Schottky}$, $j_e(X)$ and $j_i(X)$ are zero and that there is a single value of the work function for a given orifice size and select a value that minimizes the error of the absolute difference between the measured discharge current and the calculated discharge current over the entire current-flow rate parameter space, we obtained values 2.24eV, 2.2eV, and 2.36eV for the small, nominal and large cathode orifice configurations.

Plots in Fig. 11 show the quantity $J_D(\phi) - J_{D,measured}$ for every operating condition. The shape of the distribution of this plot is similar to the one that can be obtained when computing the work function per orifice plate by minimization of the standard deviation of the error, or $std(J_D(\phi) - (J_{D,measured})$, which is the proper method to calculate deviation from mean. Results shows that given the assumptions, one work function per cathode configuration is not enough to describe the cathode performance for all the operating conditions. However, they show that the difference is zero, or close to zero for a good portion of the map. A more realistic analysis that included $\phi_{Schottky}$, $j_e(X)$ and $j_i(X)$, it might be possible to identify a single work function value that could produce zero error for those portions of the map.

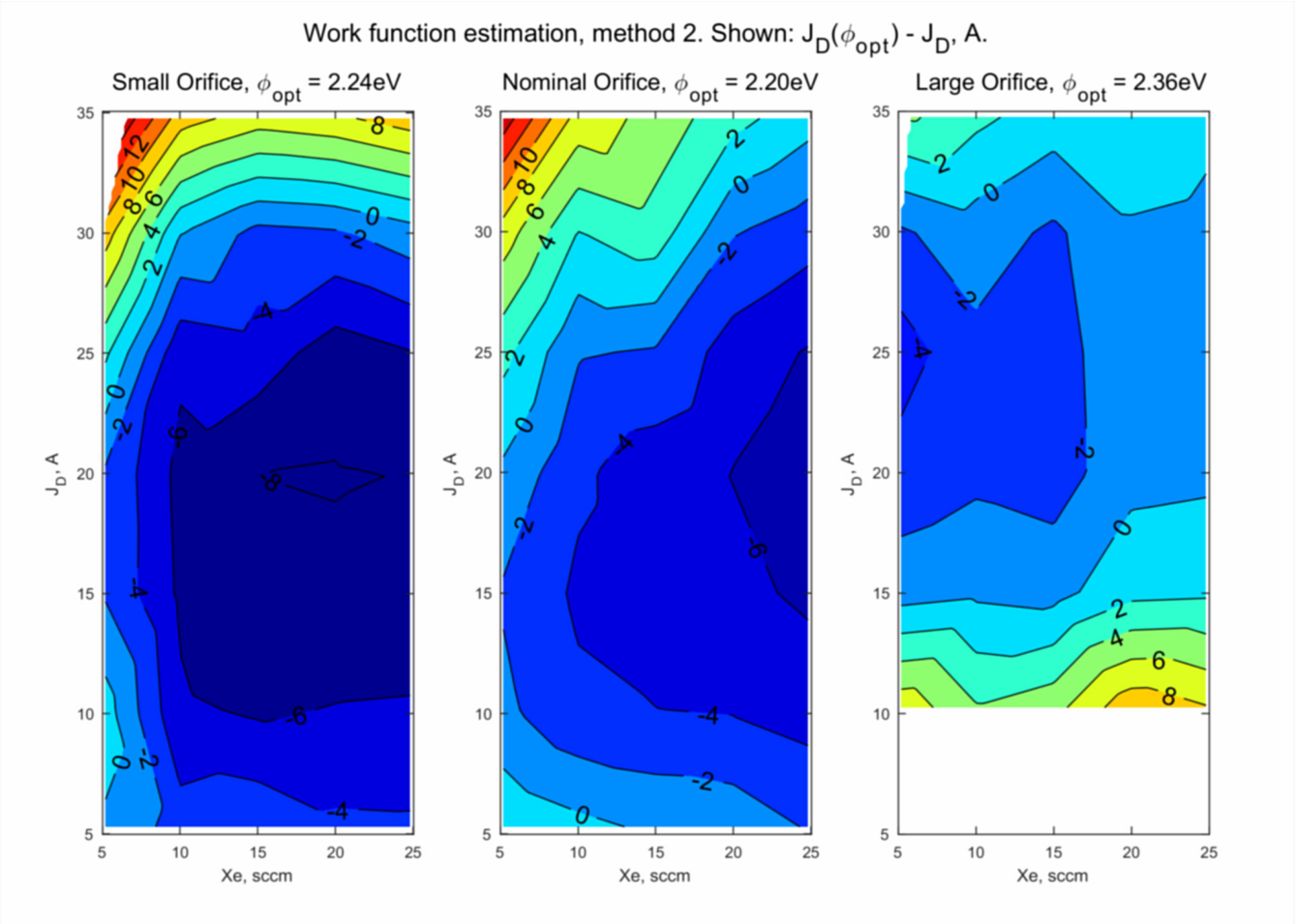

Figure 11: Computed work function with inferred insert temperature distribution, zero return current and $\phi_{Schottky} = 0$.

C. Measured work functions

We next sought to directly measure the work function and La, B and C composition of the emitting surface of an insert that had been used in the hollow cathode experiments and compare it to the estimates from the temperature data. To this end, we used the Kratos Axis Ultra XPS instrument at the Molecular Materials Research Center at the California Institute of Technology. This technique employs X-ray and ultraviolet photo-electron spectroscopy (XPS and UPS) to determine the secondary electron cutoff. Each spot was gently sputtered with an Argon ion gun at beam energy of 500V. Initially and after each sputter step the work function, C 1s, La 3d and B 1s core levels were measured. This is ongoing work, and at this point the relation between Ar ion sputtering time and penetration below the surface is not known. The calibration for the work function and the composition with absolute values is also under determination, hence, relative values are presented.

Preliminary results show a qualitative agreement in the work function profiles between the three points studied (Fig. 12a), strongly suggesting a lower work function near the emitting surface. At deeper points the work function evolves towards a constant value that we have assumed to be ϕ_{LaB_6}. The carbon levels were measured to test for the effect of surface contaminants on the work function. Results showed that the value of the work function as measured by XPS (and UPS) strongly depends on surface contamination and composition (Fig. 13). With the decrease of surface carbon contamination, the measured value of the work function drops drastically, as can be seen for spots P2 and P3 (note that for the three spots the abundance of boron is not significantly different). The carbon content for spot P1 is the highest of the three and the measured work function is significantly higher.

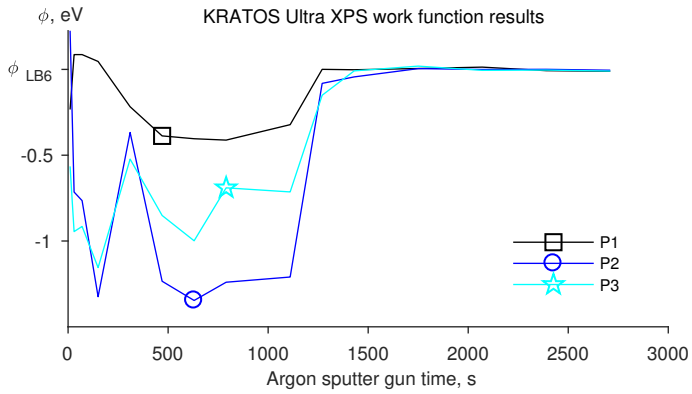

(a) Work function measurement of the insert after temperatures were collected at three different positions along the inner surface.

(b) Insert piece inside the KRATOS Ultra XPS at Caltech

Figure 12: KRATOS Ultra XPS work function analysis results as a function of sputter time.

The data suggest that the presence of carbon increases the surface work function, but nonetheless, the work function value at P3 at 500s sputter gun time is smaller than the bulk value deep inside the sample. Comparing Fig. 12a and Fig. 13 shows that the boron relative abundance and the work function for all three spots follow a similar valley type pattern between 0 and 1250s gun time. This result strongly suggests that lanthanum-rich surfaces exhibit a lower work function than the work function measured deeper in the sample, which can be assumed to be the work function of LaB_6 given the asymptotic behavior for sputter time higher than 1250s.

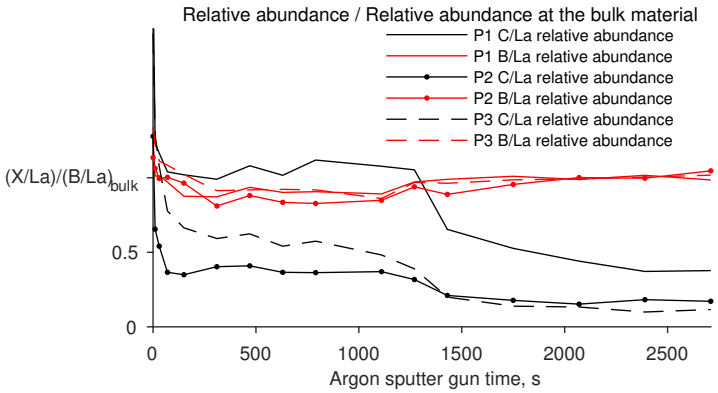

Figure 13: Relative abundance of Boron and Carbon with respect to lanthanum relative to the value at the material deepest point analyzed along three different positions along the inner surface of the insert sampled.

Importantly, note the work function peaks for spots P2 and P3 in Fig. 12a at around 350s sputter time. After the 150s measurement, the sample had to be exposed to the atmosphere for XPS maintenance. As evident in Fig. 13, the Carbon abundance at 350s for spot P3 increased, which could be the cause for the sudden increase in work function. This hypothesis is not conclusive given that spot P2 did not show an increase in the carbon composition. A complete correlation between the presence of carbon and work function increase would explain the nearly 100°C increase of steady state temperature of the cathode with the black ring deposit discussed above (Fig. 7b). Oxygen and carbon on the surface have been reported to be contaminants that effectively increase the work function by Oshima et al. [6], which is in agreement with our findings.

Fig. 13 indicated presence of carbon deep inside the insert surface. This result was not expected, as the chemical analysis certification from the manufacturer claimed that the insert was prepared from carbon-free LaB_6 powder. It is not clear whether the carbon contaminating the emitting surface comes from another component of the cathode assembly or from the press sintering process associated with the insert manufacturing. However, considering the fact that the concentration of carbon in spot P1 is higher than in P2 and P3, we speculate that the carbon may also be ionized in the plasma and returned to the insert surface by the electric field where it is preferentially deposited in a specific area.

A controlled experiment of cathode thermal transients at ignition after abrupt shuts down from steady state and repetitive ignition procedures with and without atmosphere exposure of the insert could bring more evidence on the possibility that the cathode gets contaminated with a thin film of atmospheric carbon

upon exposure, and whether carbon contamination results in higher temperature peaks during the ignition thermal transient. This would suggest a higher work function induced by the carbon film on the surface.

D. Lanthanum recycling hypothesis

The data presented above collectively suggest that lanthanum-rich surfaces that develop in a gas discharge environment could explain the apparent work function reduction at the emitting surface of the insert with respect to that of LaB_6 cathodes operated in a vacuum environment.

The source of that lanthanum could only be material evaporated from the insert itself. In order to investigate the ionization of lanthanum atoms inside the interior plasma region of the cathode, we have used the hollow cathode simulation code OrCa2D [5] to simulate the plasma. OrCa2D solves conservation laws for three species present in a partially ionized gas: electrons, singly charged xenon ions, and xenon neutrals. A time-splitting method in which all the equations are solved consecutively at every time-step is employed. Inside the cathode, the Navier-Stokes equations for neutral xenon are solved using an implicit backward Euler scheme, which includes the viscous terms. It has been shown that the flow of neutrals transitions from a low to a high Knudsen number downstream of the cathode orifice. Thus, a fluid approximation is not applicable in the cathode plume. Free molecular flow, in which neutrals move in straight paths, is assumed downstream of an axial location, typically chosen to be in the cathode orifice where the Knudsen number approaches unity. Mass and momentum continuity is preserved across the transition boundary. The Euler equations for mass and momentum of xenon ions are solved in the entire computational domain. The presence of ion momentum terms was recently included to account for the increased ion densities and currents in high-current cathodes. The effects of ionization, charge exchange and electron-ion collisions are considered in the equations and modeled as source or drag terms. Finally, the plasma parameters for electrons are determined from the solution of the electron energy equation and the combination of the current conservation equation with the vector form of Ohms law.

We simulated the nominal cathode configuration at $J_D = 25$A, $\dot{m}_{Xe}$=14.75sccm and two work functions. 2.3eV represents the upper bound of the range of possible work functions for which OrCa2D converges. Above this value, the emitted current can not satisfy charge continuity in the plasma region. 2.1eV was chosen as the lower bound because the thermionic current emitted was 62A, and that value is almost 250% J_D, which is high enough to be consider unrealistic. Results from the OrCa2d code can be used to compute the ionization mean free path (λ) for La and B (Fig. 14). Ionization cross section data from Kim [3] and Drawin [1] were used in this calculation. Results showed that for this cathode configuration and the specified work function, the mean free path for La is on the order of the orifice diameter, and therefore lanthanum atoms have a high probability of be ionized before they escape. In contrast, the mean free path for ionization of boron is an order of magnitudes bigger than the orifice diameter, thus its ionization rate is negligible.

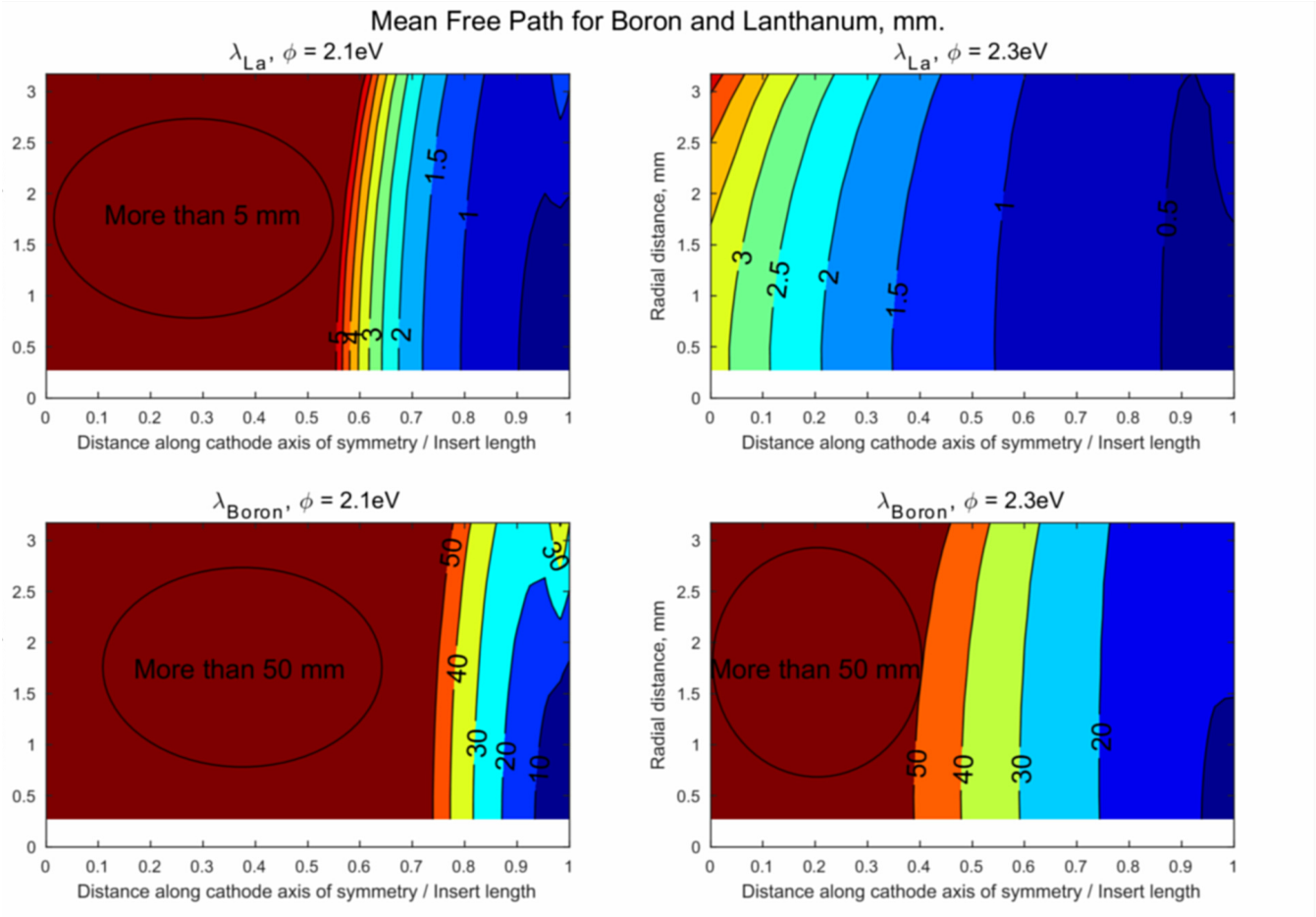

Figure 14: Mean free path estimation for boron and lanthanum in the insert region, J_D=25A, $\dot{m}_{Xe}$=14.75 sccm and nominal orifice size.

Fig. 15 shows the plasma potential along the centerline of the cathode as simulated by OrCa2D for different work functions (for the value 2.67eV, the temperature was adjusted to match the discharge current with a realistic internal plasma solution). Plasma potential can be measured with emissive and Langmuir probes with a few volts precision, which would provide an independent assessment of the work function value with 0.01 eV of precision using OrCa2D simulation results. As we increase the work function while maintaining a constant temperature distribution in the simulations, the net emission decreases according to Eq. 2, which requires a decreasing electron return current to maintain the discharge current of 25A. In this case the code raises the plasma potential so fewer electrons return to the insert from the plasma, which produces the distinctive curves shown. Results for the electron return current J_e for ϕ =2.1, 2.2 and 2.3eV are 33.7, 14.18 and 2.597A, respectively.

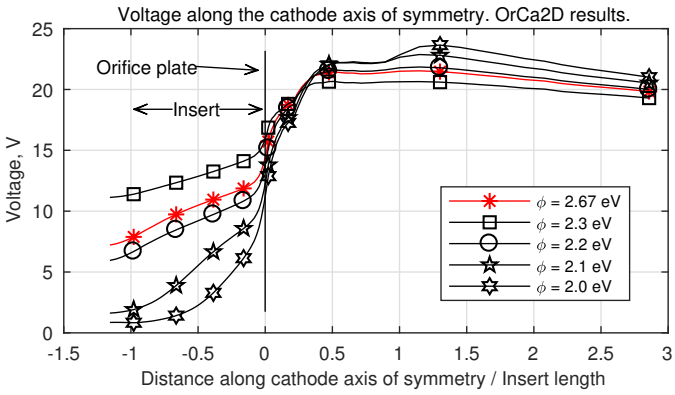

Figure 15: OrCa2D simulation results for the plasma voltage along the cathode centerline for the nominal configuration at J_D=25A and $\dot{m}_{Xe}$=14.75 sccm

With the La redeposition hypothesis, results for the thermal transient followed by the cathode with

increasing current presented in Fig. 6 and the work function prediction shown in Fig. 10 are congruent. During the first steps in current increase the insert temperature overshoots, which is consistent with cathode transitioning from a higher work function to a lower function operating point. During the first instances, right after the abrupt change in discharge current is imposed on the cathode by the power supply, the cathode is still maintaining a higher work function than the value that it will find when steady state is reached at that new operating point. The temperature will drop after those initial moments thanks to the reduction in work function that the chemistry establishes at that new operating point. We have studied all other small changes for ascending and descending discharge current and found that this explanation fits all the observations well with small discharge current steps (less than 5A).

(Figure 13 shows a boron-rich composition right at the surface of the insert. We propose the following explanation for this effect. During cathode steady state operation, redeposited lanthanum creates a gradient in composition, from pure La right at the surface (freshly redeposited), down to the bulk material composition. See black line in Fig. 16. Vaporization is the predominant mechanism immediately after extinguishing the cathode plasma, before the cathode has had time to cool. As the partial heat of vaporization is lower for the lanthanum-rich stoichiometry [7], lanthanum will evaporate away, leaving a boron-rich composition right at the surface of the insert, see red line in Fig. 16. As the cathode cools, diffusion becomes the predominant mechanism [8], bringing the surface chemistry closer to stoichiometric, thus, smoothing the differences created by the vaporization-dominated part of the cooling and the La-rich abundance gradient which define the chemical composition of the insert surface right when the cathode was shut down.

The La-B system consists of three compounds [7]: LaB_4, LaB_6, and LaB_9. Single phase LaB_6 only exists for atomic ratios of B/La between 6.0 and 6.1 (this last value is slightly dependent on temperature for the temperature range of interest for this work), and whose color in natural or incandescent light is purple. Two phases coexist from B/La ratios between 6.1 to 9. LaB_9 is been reported to appear blue [?], and therefore, in this range the surface looks blue. Two phases also coexist for B/La ratios between 4 and 6.1. In this La-rich phase, the surface appears grey [7]. This result suggest that if the insert cools down quickly, we can freeze the surface chemistry to a certain degree and by visual inspection, roughly infer the surface chemistry. In Fig. 7b the emitting surface show two distinctive colors, which suggest La-rich for the majority of the insert emitting surface and B-rich for an small area close to the orifice plate (where the carbon deposited). We could not find work function measurements for such chemistries in the literature. However, our own work function and chemical analysis suggest that La-rich chemistries have a lower work function than LaB_6. There is no definite conclusion about the impact on work function of B-rich chemistries because the carbon presence is very high in the same area where B/La concentration is higher than stoichiometric. Nevertheless, LaB_9 is considered to not have free electrons and therefore be a semiconductor [8], so a high work function value for this B-rich region is would be expected.

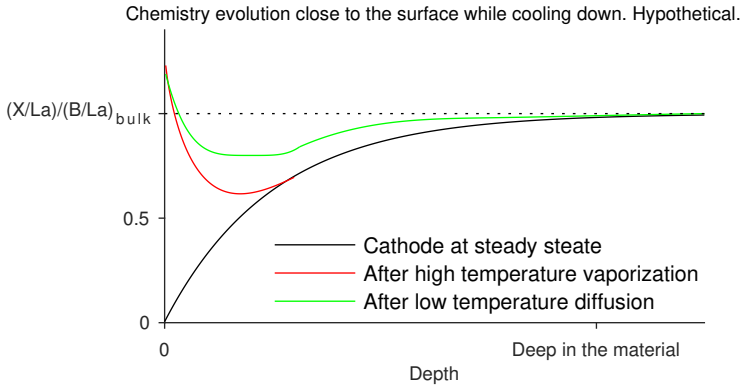

Figure 16: Hypothetical evolution of the B/La composition at the insert surface while the cathode is cooling down.

V. Conclusions

In the appendix, we discuss the thermocouple placement, accuracy and stability. We conclude from these analyses that the error introduced by the temperature measurement approach is the thermocouple accuracy plus a small temperature reduction associated with the distance between thermocouple junctions and the insert surface. Therefore, the low measured temperatures cannot be attributed to experimental error. Nonetheless, we plan to use fiber optic pyrometric techniques using a calibration source independent of thermocouples to measure the temperature profiles of the insert. This approach will remove all doubts about the temperature measurement accuracy.

Assuming that the temperature measurement was accurate, the following hypothesis could explain the low work function values. Lanthanum is evaporated from the insert constantly; its mean free path is on the order of the orifice diameter. The neutral La atoms could be ionized and pushed back to the insert surface by the electric field, making the insert emitting surface rich in lanthanum, at different amounts throughout the different operating conditions of the cathode.

The following evidence is in agreement with this hypothesis:

- The fact that the estimated work function for the large orifice plate is higher than that for the smaller ones, as lanthanum neutrals will have a shorter residence time in the region where they can get ionized.
- The lower than expected insert weight reduction in cathode insert erosion experiments [2].
- The fact that the peak temperature after re-ignition without total cool-down of the insert is lower with shallower cooling could also be explained with this model, as the concentration of La could be higher by the point of re-ignition if the cool-down was shallower. The mechanism that determines the stoichiometry after cool down plus heating is not yet clear. One hypothesis suggests that lanthanum in the most external layer of the insert evaporates easily while reheating the insert to achieve re-ignition.
- The long thermal transient for a new insert could also be explained with this model as the stoichiometry is LaB_6 when the insert is new and it will take some time for lanthanum to be deposited and diffused inside the insert, see Fig. 17.
- The dip in work function close to the insert surface that the XPS work function measurements showed.
- The dip close to the insert surface that the XPS measured for the relative abundance of boron.
- The overshoot and undershoot of the temperature transients as J_D is changed.

Further spectroscopic analyses are necessary to gain more evidence to conclude with certainty that the La recycling hypothesis is correct, but all evidence so far suggests it. Raman or infrared spectroscopy could be used in principle to measure the chemical composition of the insert inner surface while the cathode is running and has reached steady state. This is an ambitious but necessary goal to further explain the elusive mechanism that govern lanthanum hexaboride thermionic emission performance in gas discharges.

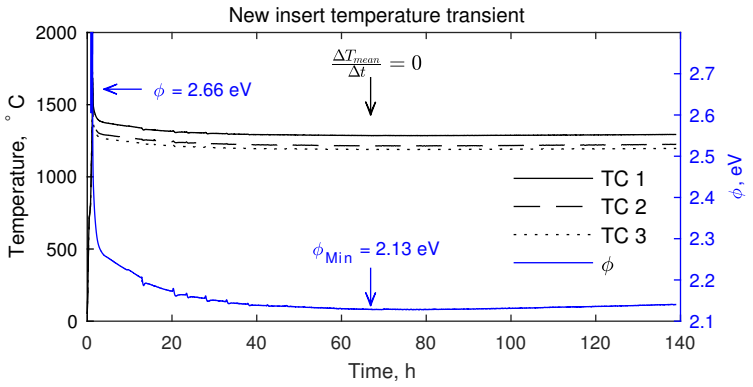

Figure 17: Thermal transient for a brand new insert at J_D=25A and $\dot{m}_{Xe}$=14.75sccm with the nominal orifice

Appendix: Validation of the results

A. Thermocouple accuracy and stability

In order to rule out any potential shifts in the performance of the thermocouples used in the cathode temperature measurements, we compared the accuracy and stability of the thermocouples used in our experiments with those of new thermocouples in an isothermal oven. Data showed that the thermocouples used in these experiments performed similarly to new ones, with accuracy within the expected range. Thus, the thermocouple calibration had not shifted during the experiments.

Boron diffusion from the insert to the tantalum sheath that protect the thermocouples was also a concern. When this happens, the tantalum becomes embrittled and cracks can appear. If that happens, boron has a direct path to contaminate the tungsten rhenium thermocouple wires, which is of a great concern as this will shift the calibration of the type C junction. Even if the tantalum sheath is not cracked, we were

concerned that boron could potentially diffuse towards the inside of the thermocouples given enough time. However, thorough examination of the thermocouples using a microscope showed that even after 1000 hours of operation they did not develop cracks. Taken together with the accuracy agreement between new and used thermocouples discussed above, these data suggest that in the presence of the tantalum sheath and for the time frame of the observations, boron does not diffuse through the tantalum.

With the objective of minimizing the heat conduction away from the insert through the thermocouples we further tested whether the tantalum sheath could be removed from the thermocouples. However, we found that in the absence of the tantalum sheath the thermocouple calibration shifted rapidly and abruptly. We propose that the calibration shift is possibly due to boron diffusion in the tungsten rhenium wires. In addition, the alumina structure disappeared during this test, and the thermocouple wells in the insert whitened. Alumina tends to fill the pores of the sintered insert. Given these issues, we concluded that tantalum sheath removal is not feasible.

B. Artificial cooling

COMSOL thermal simulations were used to study possible temperature deviation due to the installation of the thermocouples. The thermal flux distributions on the insert from the OrCa2D simulations for the cases 2.1 and 2.3 eV were used as the heat flux boundary condition on the insert exterior, see Fig. 18. The boundary condition for the inner surface was the measured temperature distribution from the thermocouples data. First, the insert temperature distribution was calculated with the aforementioned boundary conditions without any thermocouples. The temperature at six points in the simulation domain was extracted at the point where the thermocouple junctions would be and 1.5 mm away from the junctions, into the insert material. Assessment with the insert perforations showed a difference with respect to the non-perforated insert at the six points of less than 2°C for both thermal flux distributions.

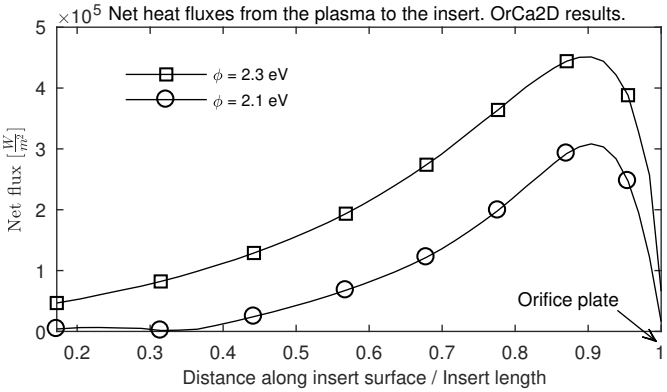

Figure 18: Thermal heat fluxes along the insert of the cathode at J_D=25A and $\dot{m}_{Xe}$=14.8sccm with the nominal orifice.

Following this analysis, the insert with the three inserted thermocouples was studied. Thermocouples were simulated as solids with thermal behavior equal to the real multicomponent structures. The thermocouples stick out of the insert 150 mm, at which point a 100°C temperature boundary condition was applied. This value was obtained from a real thermocouple monitoring the temperature at that location during experiments. The given value was the coldest temperature point that was measured during testing. Perfect thermal contact was simulated between the insert and the thermocouples. The thermocouples were allowed to drive heat out of the insert and the value was recorded. Ambient temperature with which the thermocouples could exchange heat due to radiation was set to 1000, 900, 700, and 500°C . Non-radiating thermocouples were also simulated. The results from this experiment at the six points with respect to the intact insert agree within 0.6°C for both thermal fluxes. The total amount of heat that the three thermocouples drive out of the insert was less than 15% of the heat input to the insert from the plasma, less than 4.2W per thermocouple. If the thermocouples rely on radiation to measure the heat transfer inside the insert, with enough heat flux output, they can definitely measure lower than local temperatures. In order to avoid that, a spring loaded thermocouple approach was built to ensure good thermal contact with 26.02 lb./in stiffness constant springs. Temperatures were measured with this approach at J_D=25A and $\dot{m}_{Xe}$=14.75sccm and they agree with the data obtained earlier.

Acknowledgments

The support of the joint NASA GRC and JPL development of HERMeS by NASA's Space Technology Mission Directorate through the Solar Electric Propulsion Technology Demonstration Mission project is gratefully acknowledged. Portions of the research described in this paper were carried out at the Jet Propulsion Laboratory, California Institute of Technology, under a contract with the National Aeronautics and Space Administration. Research was in part carried out at the Molecular Materials Research Center of the Beckman Institute of the California Institute of Technology. This work was supported through the Office of Science of the U.S. Department of Energy (DOE) under award no. DE SC0004993 to the Joint Center for Artificial Photosynthesis, a DOE Energy Innovation Hub.

References

[1] H. W. Drawin. Zur formelmigen darstellung der ionisierungsquerschnitte gegenber elektronensto. 164: 513–521, 1961. ISSN 1434-6001. doi: 10.1007/bf01378424.

[2] J. E. P. Giulia Becatti, Dan M. Goebel and P. Guerrero. Life evaluation of a lanthanum hexaboride hollow cathode for high power hall thrusters.

[3] Y.-K. Kim and P. M. Stone. Ionization of boron, aluminum, gallium, and indium by electron impact. 64. ISSN 1050-2947. doi: 10.1103/physreva.64.052707.

[4] W. H. Kohl. Handbook of materials and techniques for vacuum devices / Walter H. Kohl. pages XVI, 498 p. :, 1967.

[5] A. L. Ortega, I. G. Mikellides, and B. Jorns. First-principles modeling of the iat-driven anomalous resistivity in hollow cathode discharges ii: Numerical simulations and comparison with measurements, 2016.

[6] C. Oshima, E. Bannai, T. Tanaka, and S. Kawai. Thermionic work function of lab6single crystals and their surfaces. 48:3925–3927, 1977. ISSN 0021-8979. doi: 10.1063/1.324266.

[7] E. Storms and B. Mueller. Phase relationship, vaporization, and thermodynamic properties of the lanthanum-boron system. 82:51–59, 1978. ISSN 0022-3654. doi: 10.1021/j100490a014.

[8] E. K. Storms and B. A. Mueller. A study of surface stoichiometry and thermionic emission using lab6. 50: 3691–3698, 1979. ISSN 0021-8979. doi: 10.1063/1.326323.